Cross-flow Effect on Flow and Heat Transfer Characteristics of Impinging Jets in a Confined Channel

Makatar Wae-hayee, Perapong Tekasakul and **Chayut Nuntadusit**

Department of Mechanical Engineering, Faculty of Engineering, Prince of Songkla University, Hat Yai Songkhla 90112, Thailand

Manuscript received April 28, 2014
Revised May 15, 2014

ABSTRACT

The flow and heat transfer characteristics of impinging jets with cross-flow effect were investigated for single impinging jet, a row of impinging jets and an array of impinging jets. For case of single impinging jet and a row of impinging jets, the cross-flow was introduced in wind tunnel and flew cross the single jet and row of jets. The jet velocity was fixed corresponding to Re=13400, and cross-flow velocity were varied corresponding to velocity ratio (jet velocity/cross-flow velocity), VR=3, 5 and 7. For array of impinging jets, the jets from 4 rows × 6 columns was studied in the confined channel for inline and staggered arrangement. The jet Reynolds number for each orifice was fixed at Re=13,400. The jet-to-jet distance was fixed at S/D=3, and jet-to-plate distance was fixed at H/D=2 (D is 13.2 mm of orifice diameter). For single impinging jet and row of impinging jets, it was found the local heat transfer at impingement regions for the high cross-flow velocity are higher than that the low one. This result attributes from high momentum that impinge on target surface and high turbulence intensity distribution on the surface. For array of impinging jets, it was found that the heat transfer rate of jet with inline arrangement is higher than those the staggered one. The cross-flow can easily pass through the gaps between the rows of inline jets, whereas it appears to be directly blocked by the downstream jet for the case of staggered arrangement.

Keywords*: Impinging jets, Cross-flow, Heat transfer characteristics, Flow characteristics, Thermochromic liquid crystal, Flow visualization, CFD*

1. INTRODUCTION

Jet impingement is a heat transfer enhancement technique which is widely applied in thermal equipment. It has also been used in industrial processes for heating, cooling and drying. Since the heat transfer rate is very high at the area where the jet directly impinges on, it provides rapid cooling or heating on the local heat transfer area. When high and uniform heat transfer rate is required over the entire surfaces, multiple impinging jets or array of impinging jets are applied such as combustor chamber wall and gas turbine blade cooling, steel and glass quenching and textile and paper drying [1] – [5].

An important factor affecting on flow and heat transfer characteristics of multiple impinging jets in confined space is cross-flow. Cross-flow is defined as fluid which flow cross to the jet impingement flow. In case of multiple impinging jets in a confined space, the spent jet is accumulated from upstream to the downstream end of the channel. The flow rate or velocity of the cross-flow is thus increased from upstream to the downstream of the channel. Consequently, impinging jets tend to deflect to cross-flow direction and impinge on impingement surface with lower momentum due to mixing with cross-flow, and their heat transfers are significantly reduced by the cross-flow [4], [5].

The effects of cross-flow on flow and heat transfer characteristics for multiple impinging jets were preliminarily investigated. Katti and Prabhu [5] experimentally investigated the influence of jet-to-jet distance in the range of $2 \leq S/D \leq 6$ and jet-to-plate distance in the range of $1 \leq H/D \leq 3$ (D is nozzle diameter) on heat transfer rate of array of impingement jets with in-line arrangement in confined duct with orifice nozzles. Their results suggested that cross-flow significantly affected the heat transfer rate of impingement jets in downstream. Florschuetz et al. [4] developed the Nusselt number correlation for both inline and staggered arrangement using orifice nozzles with a jet-to-jet distance and a jet-to-plate distance in the range

of $4 \leq S/D \leq 15$ and $1 \leq H/D \leq 6$, respectively. Brizzi et al. [2] showed the flow and temperature patterns on the impingement surface of array of jets from orifice nozzle with an inline arrangement under jet-to-plate at H/D=2 and jet-to-jet distance S/D=4. Their findings indicated that the flow patterns corresponded to the temperature distributions.

However, flow characteristics of an impinging jet under cross-flow and the interactions between adjacent impinging jets and inherent cross-flow are rarely discussed. So, the investigations are usually performed by applying simulated cross-flow through a single impinging jet in a wind tunnel. Barata and Durao [6] studied impinging jet flow from long pipe nozzle discharging through a cross-flow using Laser-Doppler measurement under constant jet-to-plate distance of H/D=5 and velocity ratio in the range of $30 \leq VR \leq 73$. The size of upstream ground vortex was found to be smaller when the cross-flow velocity increased. Goldstein and Behbahani [7] and Bouchez and Goldstein [8] examined impinging jet from pipe nozzle impinging in simulated cross-flow with jet-to-plate distance of H/D=6 and 12 and velocity ratio in the range of $3.37 \leq VR \leq 17.50$. They found that the heat transfer rate by an impinging jet at stagnation point decreased with increasing cross-flow velocity. Heo et al. [9] used numerical simulation to predict the flow and heat transfer characteristics of an inclined impinging jet from long pipe impinging into the cross-flow under a jet-to-plate distance of H/D=6 and velocity ratio at VR=7.98.

According to the previous works as reviewed, a single and multiple impinging jets with effects of cross-flow were studied separately with identical parameters. To identify the cross-flow effect on impingement flow, the investigation parameters (a jet-to-plate distances, nozzle configuration and velocity ratio) of a single impinging jet with simulated cross-flow should be the same with the investigation parameters of an array of impinging jets in a confined channel. In this study, effects of cross-flow on flow and heat transfer characteristics of single and multiple impinging jets under the same investigation parameters were studied.

The aim of this article is to investigate the effect of cross-flow on flow and heat transfer characteristics of a single impinging jet, a row and an array of impinging jets at small jet-to-plate distance H/D=2. To explain the effect of cross-flow on flow and heat transfer characteristics of a single impinging jet, a row and an array of impinging jets, orifice nozzle, jet-to-plate distance and jet Reynolds number were identically assigned.

2. EXPERIMENTAL MODELS AND PARAMETERS

2.1 Experimental Models

Experimental models are categorized with three types; the single impinging jet and the row of jets impinging on the inner wall of wind tunnel under simulated cross-flow as shown in Fig. 1, and array of impinging jets with inline and staggered arrangement as shown in Fig. 2. The air jets discharge from round orifices on one side of wind tunnel and impinge on wind tunnel wall on the opposite side. For the single impinging jet and the row of impinging jets, the cross-flow was simulated by introducing through the test section of wind tunnel. For the case of array of impinging jets, the cross-flow is generated by accumulation of the spent jet (jet after impinging) in the upstream region which flows out to the exit at the other end of the confined channel as shown in Fig. 2(a). The jet configurations, for the inline and staggered arrangement, consist of 24 jet holes distributed in 6 columns and 4 rows as shown in Fig.2(b) and 2(c). [9] – [11]

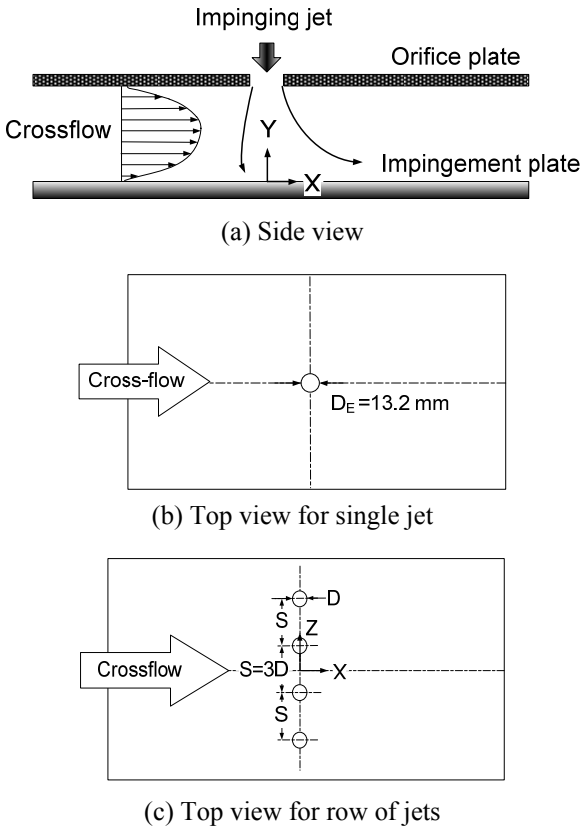

Fig. 1 *Experimental models for single impinging jet and a row of impinging jets with cross-flow.*

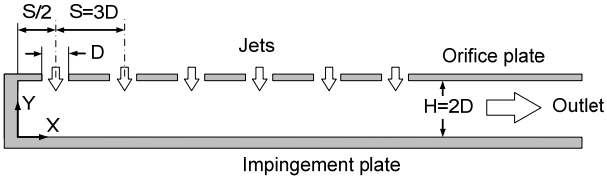

(a) Side view

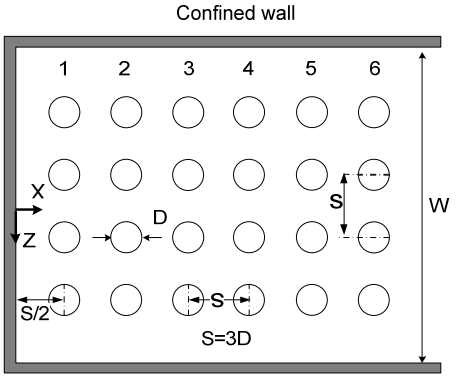

(b) Top view for inline arrangement

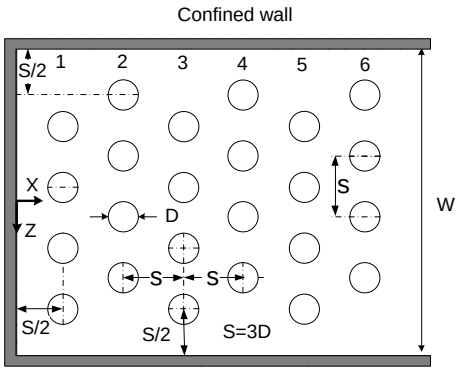

(c) Top view for staggered arrangement

Fig. 2 *Experimental model for array of impinging jets in confined channel.*

2.2 Experimental Parameters

For case of single impinging jet and row of impinging jets, the effect of the cross-flow velocity on the flow and heat transfer characteristics was investigated by varying the cross-flow velocity corresponding to three different velocity ratios (jet velocity to cross-flow velocity measured at the center of channel) *VR*=3, 5 and 7 while the jet velocity was kept constant at 15 m/s corresponding to *Re*=13,400. The diameter of each round orifice, having smooth square-edge nozzle drilled on a plate of 2-mm thickness, is D=13.2 mm. The jet-to-plate distance was *H/D*=2, and the jet-to-jet distance for a row of impinging jets was fixed at *S/D*=3.

For the array of impinging jets, the in-line and staggered arrangement were examined. Both jet arrangements have same array of 6×4 jet holes; 6 columns in the streamwise direction and 4 rows in the spanwise direction of confined channel. Both arrangements have a constant jet-to-jet distance of *S/D*=3 and jet-to-plate distance of *H/D*=2. The orifice geometry was the same as used in single impinging jet and row of impinging jets. The experiments were carried out at jet Reynolds number of *Re*=13,400.

3 MEASUREMENT METHODS

3.1 Heat Transfer Measurement

Air with a constant temperature is discharged through the orifice plate and impinges upon the heat transfer surface. The heat transfer surface, made of stainless steel foil (30 μm thick), is attached with a Thermochromic Liquid Crystal (TLC) sheet on the rear side of the impingement surface for measuring the temperature distributions. The stainless steel foil is stretched between two of copper bus bars. The heat transfer surface is heated by a DC power supply that can supply an electrical current up to 50 A through the copper bus bars. Electrical energy dissipated in the stainless steel foil can be calculated with the Joule effect equation:

$$\dot{q}_{joule} = \frac{I^2 R}{A} \tag{1}$$

where I is the electrical current, R is the thermal resistance of the stainless steel foil and A is area of stainless steel foil.

The local heat transfer coefficient due to the forced convection of the impinging jets, h, can be evaluated from:

$$h = \frac{\dot{q}_{joule} - \dot{q}_{loss,rad} - \dot{q}_{loss,conv}}{T_w - T_j} \tag{2}$$

where $\dot{q}_{loss,rad}$ and $\dot{q}_{loss,conv}$ are the heat losses from TLC sheet on the impingement surface to the environment by radiation and natural convection, respectively, T_w and T_j are the wall temperature obtained from TLC sheet and jet temperature measured in the jet chamber with thermocouple type T.

Heat loss due to radiation can be calculated from:

$$\dot{q}_{loss,rad} = \sigma \varepsilon_{TLC} (\overline{T_w}^4 - T_s^4) \quad (3)$$

and heat loss due to natural convection can be calculated from:

$$\dot{q}_{loss,conv} = \overline{h_c}(\overline{T_w} - T_s) \quad (4)$$

where σ is the Stefan-Boltzman constant, ε_{TLC} is the emissive coefficient of the TLC sheet, T_s is the ambient temperature, and $\overline{h_c}$ is the average natural heat transfer coefficient calculated from the natural convective heat transfer from the heat transfer surface to the surrounding.

The local Nusselt number can be calculated from:

$$Nu = \frac{hD}{k} \quad (5)$$

where D is diameter of round orifice, and k is thermal conductivity of air jet.

3.2 Flow Visualization

The flow pattern on the impingement surface was visualized by using the oil film technique. The oil film was prepared by mixing liquid paraffin, titanium dioxide powder and oleic acid. The transparent plastic plate was employed as an impingement surface instead of stainless steel foil and was uniformly painted with the oil film on the plastic plate. During the experiment, the oil film pattern on the impingement surface was moved by the impinging jet flow and recorded with digital video camera.

3.3 Numerical Simulation

The flow characteristics of the impinging jets with cross-flow effect was investigated by employing a 3-D numerical simulation with the ANSYS ver. 13.0 (Fluent). The calculation which was based on a finite volume method was adopted to solve the Reynolds averaged continuity equation, Navier-Stokes equation and energy equation. A numerical model was the same as the experimental model. The boundary conditions were identically specified to the experimental conditions. The details of the numerical simulation were specified in the previous studies [9] – [11]. A SST $k-\omega$ turbulence model was applied for turbulent flow prediction due to its high accuracy and moderate computational cost [12]. This turbulence model has also been employed to accurately predict flow and heat transfer characteristics of an impinging jet under the cross-flow [13], [14]. A solution method was based on a SIMPLE algorithm with a second order upwind for all spatial discretization.

4. RESULTS AND DISCUSSION

4.1 Single Impinging Jet in Simulated Cross-flow

Fig.3 shows streamlines of a single impinging jet in a cross-flow on X-Y plane passing the center of jet exit (Z/D=0). The jet from the orifice impinges on the surface and then flows on the impingement surface as a wall jet in the upstream and downstream directions of the cross-flow. The wall jet in upstream direction interacted with the cross-flow and induced a large ground vortex. The size of this ground vortex decreased with increasing cross-flow velocity (decreasing VR=7 to 5). The ground vortex could not be seen for the case of a high cross-flow velocity (VR=3). As seen from Fig. 3, some parts of cross-flow are induced by the jet flow to impinge on the surface for case of VR= 5 and 7.

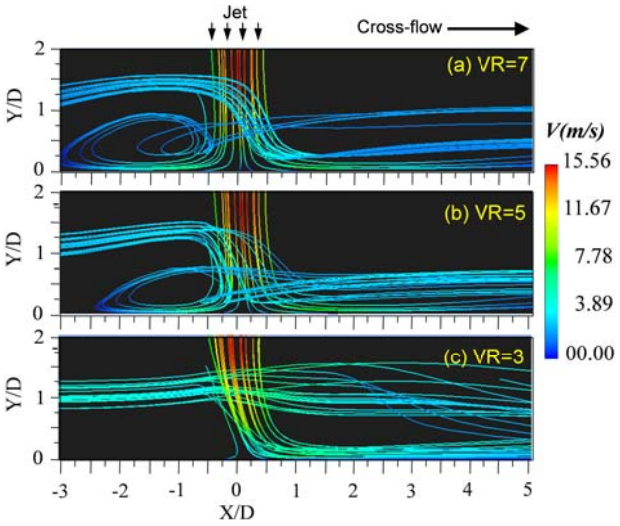

Fig. 3 *Streamlines of a single impinging jet in cross-flow on X-Y plane passing the center of jet exit (CFD results, Z/D=0)*

The velocity vectors and velocity contours in the Y-component on Z-X plane at 1.5-mm above the impingement surface are shown in Fig.4. The Y-component velocity represents the velocity in the direction normal to the impingement surface. The positive velocity means the flow is on direction impinging on the surface. The negative velocity means the flow is in a direction away from the surface. In Fig.4, the region with high and positive velocity corresponds to the jet impingement region and the line

with a negative velocity corresponds to the upwash flow due to the ground vortex in the upstream region. When the cross-flow velocity increases, the impingement region becomes smaller and shifts downstream, especially, the case of a high cross-flow velocity at VR=3 (Fig.3(c)). The location of upward flow moves more close to the impingement region when the cross-flow velocity is increased. This is due to the significant jet deflection caused by the cross-flow.

The flow visualization on the impingement surface captured by the oil film technique is shown in Fig.5. The black region is the impingement region where the oil film was completely removed while the grey region around the impingement region is the wall jet region where the oil film partly removed from wall. The small white region surrounded by the black region (impingement region) represents the stagnation point bounded by the impingement region. The visualization shows that impingement region (black region) becomes smaller and the wall jet (grey region) upstream of the impingement region is more contracted while the wall jet in the downstream of impingement region is more elongated to the downstream region as the cross-flow velocity increases. This corrresponds with flow patterns on Fig.4..

Temperature distributions on the impingement surface for all VR are shown with a color pattern on the TLC sheet in Fig. 6. The region with low temperature corressponds to the impingement region with a high heat transfer rate. The area with a higher temperature corresponds to region with a lower heat transfer rate. The area of the impingement region with a red color tend to increase with cross-flow velocity (decreasing from VR=7 to 3), while the area of the wall region with a green color tends to decrease in the upstream region and increase in downstream region when the cross-flow velocity is increased. The temperature patterns coincide with the flow patterns on the impingement surface as shown in Fig. 4 and Fig. 5.

The Nusselt number distributions along the cross-flow direction at $Z/D=0$ obtained from the numerical simulation are shown in Fig.7(a). These results agree well with the heat transfer characteristics from the TLC sheet in Fig. 6. The Nusselt number in upstream region ($X/D<0$) becomes lower when cross-flow velocity increases. This corresponds to the contraction of the wall jet and impingement region in the upstream as shown in Fig. 5.

Fig.7(b) presents the distributions of the Y-component of the velocity in the direction normal to the impingement wall) at 1.5-mm above the impingement surface. When the cross-flow velocity is increased, the peak velocity in the jet impingement region tends to decrease and shift to downstream region, particularly for the case of VR=3.

The distributions of the turbulence kinetic energy at 1.5-mm above the impingement surface are shown in Fig.7(c). At low and medium cross-flow velocity (VR=7 and 5), the regions with high turbulence kinetic energy are detected in both the upstream and downstream regions of the wall jet, and the high intensity region of the upstream wall jet is larger than that of the downstream one. In addition, the turbulence kinetic energy in stagnation region is very low for the case of small impingement distance [15, 16]. As the cross-flow velocity increases to VR=3, the peak of turbulence kinetic energy in the upstream wall jet becomes smaller, and the turbulence kinetic energy in the stagnation region becomes larger than the case of VR=5 and 7.

The peak of Nusselt number for case of VR=3 becomes larger than case of VR=5 and 7. This can be explained by high impingement velocity and high turbulence kinetic energy. However, The Nusselt number peak for case of VR=5 and 7 is lower than case of VR=3. This is due to small turbulence kinetic energy. This is different from what was found at a large jet-to-plate distance ($H/D>2$) [4], [15].

4.2 Row of Impinging Jets in Simulated Cross-flow

The velocity vectors and velocity contours on the Z-X plane above the impingement surface of 1.5-mm are presented in Fig.8. It should be noted that these figures show the center of two impinging jets within the row of impinging jets. The impingement region is found in a semi-circular shape for the case of VR=7. This is different from the case of a single impinging jet in cross-flow. It is due to the row of impinging jets blocking the simulated cross-flow in the wind channel and the cross-flow effect becomes more significant.

The lines of negative velocity (upward flow) can be clearly observed in the upstream regions of jet impingement which is the same as the case of a single impinging jet. In addition, the lines of negative velocity contour are detected in the middle region between adjacent impingement regions. It is due to the interaction between adjacent impinging jets. However, this area becomes smaller when the cross-flow velocity increases due to the strong mixing of upward flow and cross-flow.

The flow visualizations on the impingement surface by the oil film technique are shown in Fig.9. This figure shows the oil film patterns comparisons of the effect of cross-flow. These oil film patterns agree well with those of the simulated results in Fig.8. The impingement regions shift to the downstream and the wall jet regions elongate to downstream when increasing the cross-flow velocity. The oil film between the impingement regions is partly removed due to the strong collision between the wall jets from adjacent impinging jets.

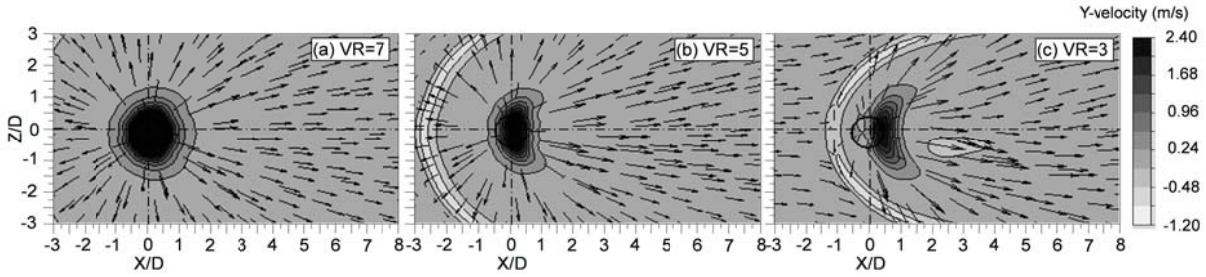

Fig. 4 *Velocity vectors and contours of Y-component velocity on Z-X plane at 1.5-mm above the impingement surface for a single impinging jet in cross-flow (CFD results, the marked circles represent the position of the orifice.) [9].*

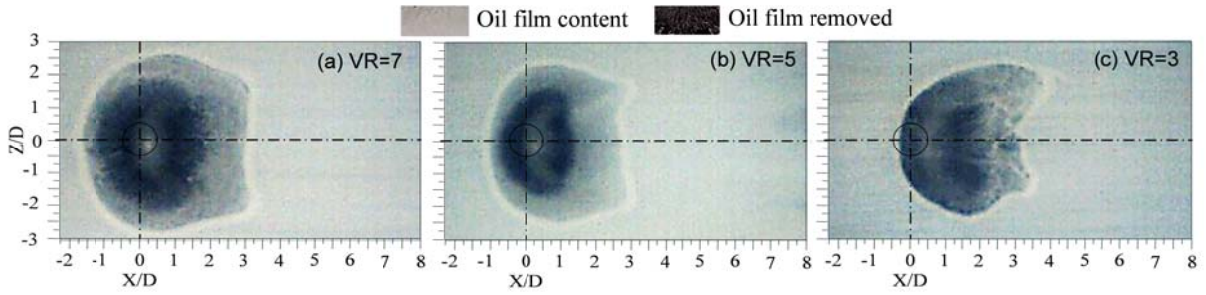

Fig. 5 *Oil film patterns on the impingement surface for a single impinging jet in cross-flow.*

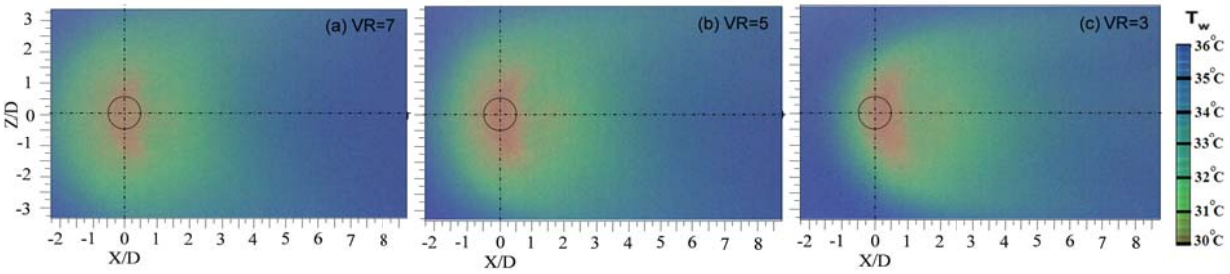

Fig. 6 *Thermal visualization on the impingement surface for a single impinging jet in cross-flow (T_j=27 ^{o}C, Re =13,400, $\dot{q}_{joule}$=429 W/m^2).*

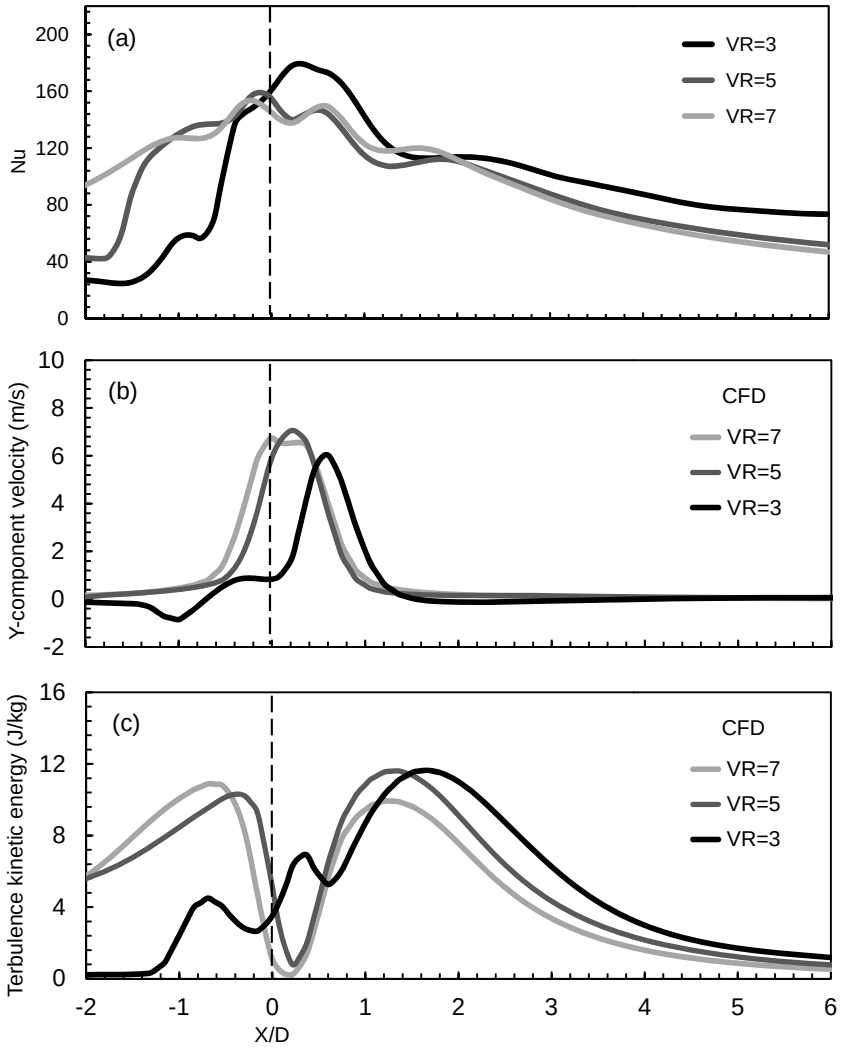

Fig. 7 *Comparisons between Nusselt number, Y-component velocity and turbulence kinetic energy on X-axis obtained from CFD results for a single impinging jet in cross-flow (a) Nusselt number; (b) Y-component velocity (1.5-mm above the impingement surface) and (c) turbulence kinetic energy (1.5-mm above the impingement surface).*

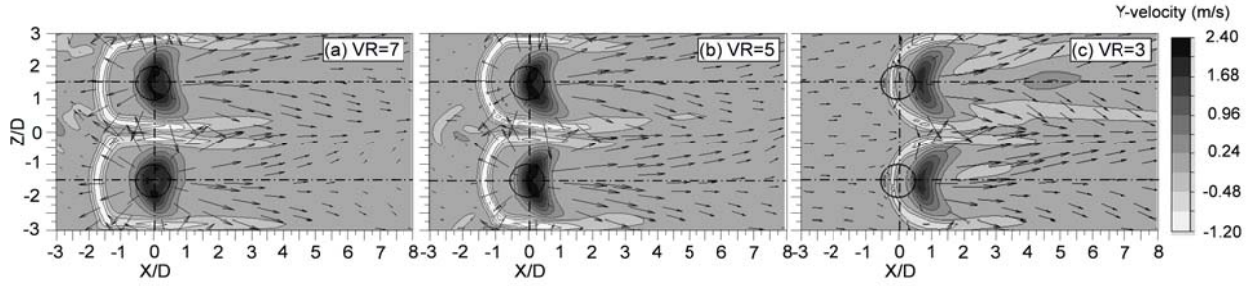

Fig. 8 *Velocity vectors and contours of Y-component velocity on Z-X plane at 1.5-mm above the impingement surface for a row of impinging jets in cross-flow (CFD results, the marked circles represent the position of the orifice.) [10].*

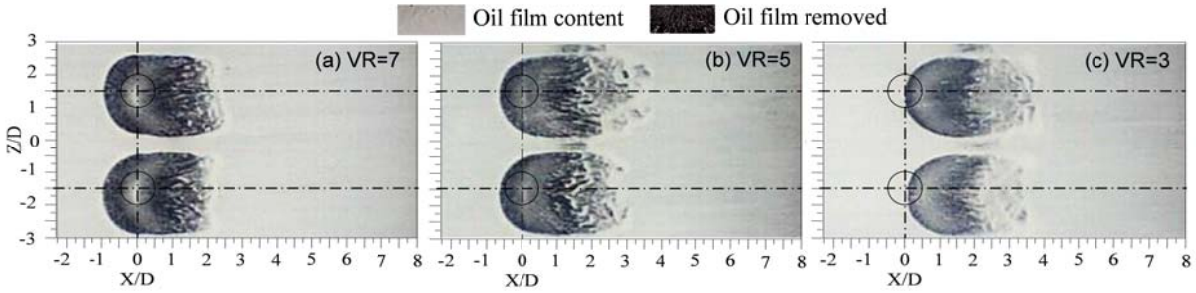

Fig. 9 *Oil film patterns on the impingement surface for a row of impinging jets in cross-flow.*

Fig. 10 show the variation of flow patterns on the Y-Z plane at different downstream locations for a row of impinging jets in cross-flow at VR=3 (large cross-flow velocity) and 7 (small cross-flow velocity). For case of small cross-flow velocity (VR=7), the jet flows from row of orifices impinge on the surface and the wall jets from adjacent impinging jets collide and flow upward from the surface, called "upward fountain" [17], [18] in plane X/D=0.0. Then, the upward fountains impinge the upper wall and flow on the upper wall before entraining to the jet flow again. As it moves downstream, the circulation flows between the impinging jets are still driven by the upward fountain flow. However, the circulation flows become weaker due to small cross-flow velocity.

For case of large cross-flow velocity (VR=3), The jet flows from the row of orifices are deflected by cross-flow before reaching the impingement surface. As shown in plane at X/D=0.5, the cross sections of jet flows are found near the impingement surface. However, the upward fountains are found due to the collision of adjacent jet flows in the spanwise direction. A pair of circulation flows are generated for each jet from plane at X/D=1.0. From plane at X/D=3.0, some circulation flows disappear and the remaining circulation flows are drived by upward fountains.

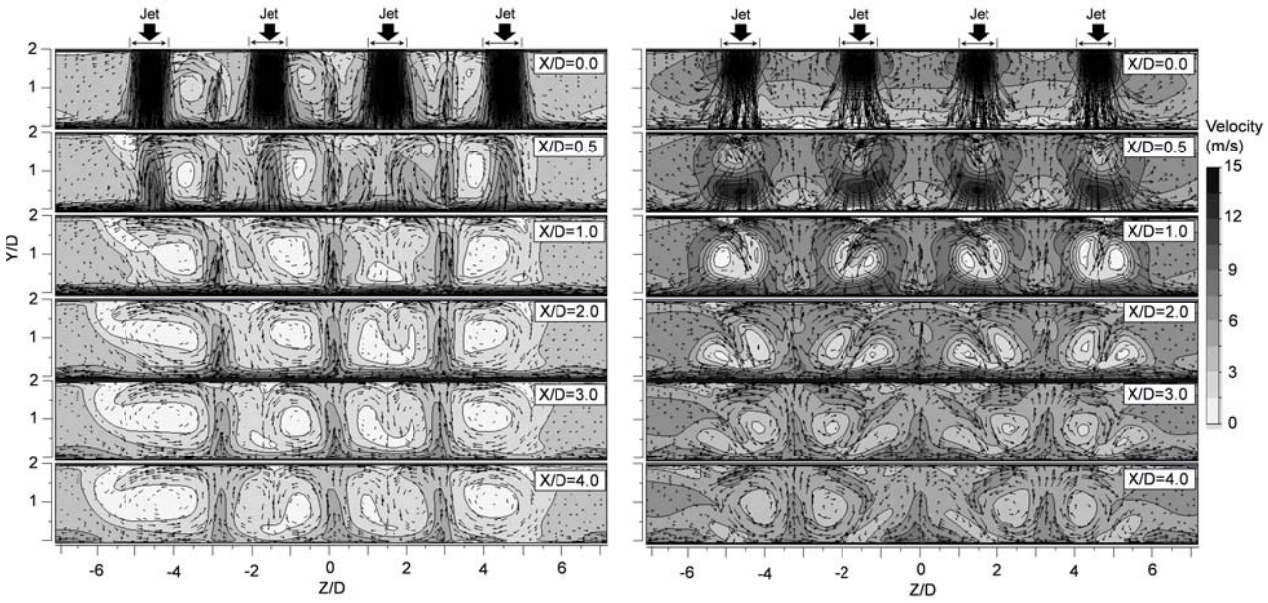

Fig. 10 *Variation of flow patterns on Y-Z plane along downstream direction for a row of impinging jets in cross-flow at VR=7 (left) and VR=3 (right).*

Fig.11 shows the thermal visualization on the impingement surface for a row of impinging jets in cross-flow using TLC sheet. The heat transfer enhancement (area with red color) in the jet impingement region is found when the cross-flow velocity is increased corresponding to VR=3. In

addition, the heat transfer enhancement in the region between the adjacent impinging jets could be seen for small and medium cross-flow velocities (VR=5 and 7).

Fig.12 shows the distributions of the local Nusselt number along the line in X direction between a single impinging jet and a row of impinging jets in cross-flow. The results are obtained from the image processing of color on TLC sheet. The peak of Nusselt number shifted to downstream for row of impinging jets when compares to case of a single impinging jet in cross-flow. The Nusselt number on upstream side for the case of the row of impinging jets is lower than case of single impinging jet in cross-flow. This is due to strong cross-flow effect for the row arrangement. In contrast, the Nusselt number on the downstream side for the case of the row of impinging jets is higher than case of the single impinging jet. This may be as a resulof the circulation flows within channel induced from interaction between the adjacent impinging jets promoting the heat transfer rate in the downstream region.

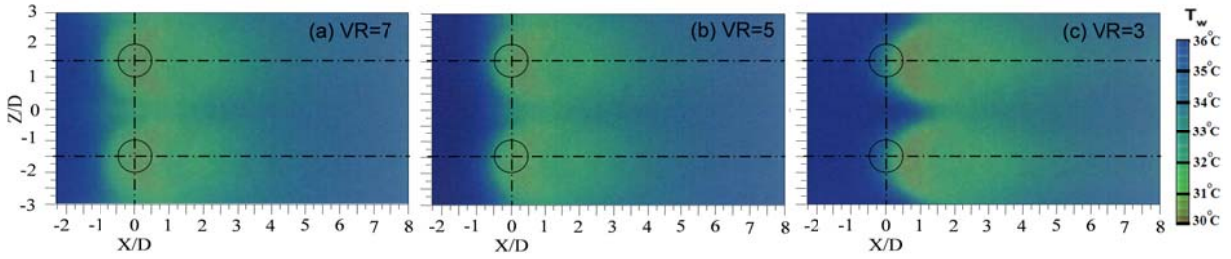

Fig. 11 *Thermal visualization on the impingement surface for a row of impinging jets in cross-flow (T_j=27 °C, $\dot{q}_{joule}$ = 366 W/m^2).*

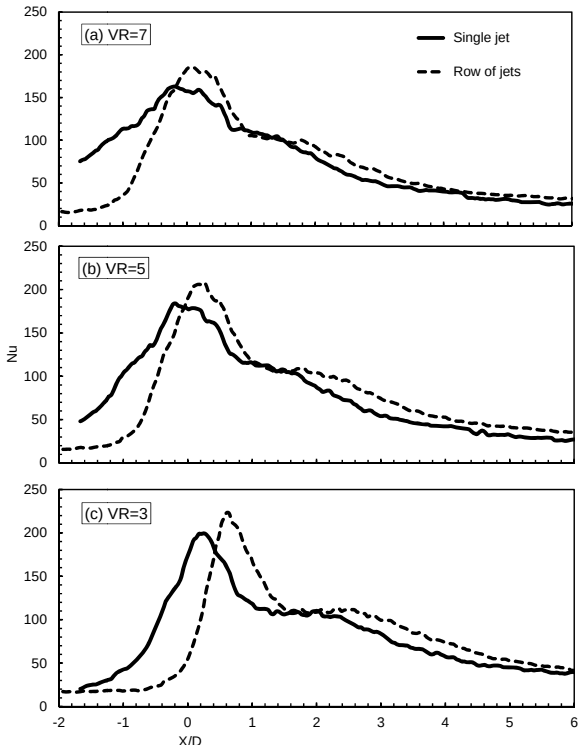

Fig. 12 *Comparison of the Nusselt number distributions on the X-axis between a single impinging jet and a row of impinging jets in cross-flow (Experimental results, T_j=27°C).*

4.3 Array of Impinging Jets in a Confined Channel

The flow characteristics of the impinging jets on the Z-X plane near the impingement wall (1.5-mm above the wall) for *Re*=13,400 are shown in Fig.13. The figure show for two rows of impinging jets in the center of the array. The impingement velocity and the velocity vector near the impingement surface are shown. The regions with high impingement velocities are corresponding to the impingement regions of impinging jets.

The impingement regions in the case of the in-line arrangement were clearly shifted towards the downstream direction due to the effect of the cross-flow as shown in Fig. 13(a). The displacement of each impingement region from the orifice location increases as it moves downstream. This is due to the accumulating cross-flow from upstream impinging jets. The cross-flow effect increases for the downstream impinging jets. The jet from the orifice is more deflected by the cross-flow. The impingement region changes its shape from circular to semi-circular as it moves downstream.

For the case of the staggered arrangement, the impingement velocity in the impingement region decreases as it moves downstream as shown in Fig. 13(b). The impingement regions for orifice jets in column No. 5 and No. 6 cannot be identified due to strong collision of the crossflow on the jets before impingement.

Flow visualization on the impingement surface using the oil film technique is shown in Fig.14. The grey region where the oil film is partly removed corresponds to the impingement region. The flow patterns of both the in-line and staggered arrangements are agree well with simulation results in Fig. 13.

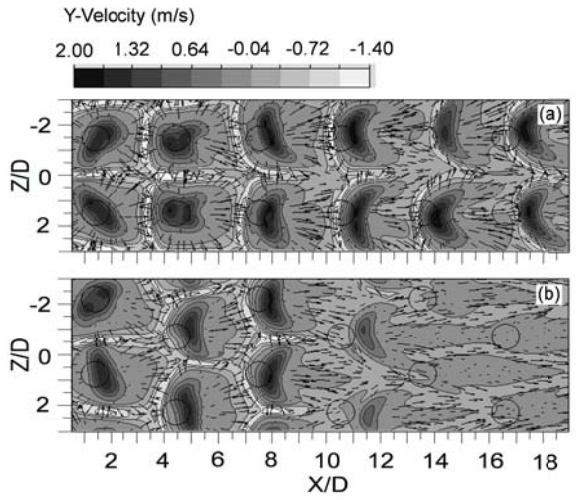

Fig. 13 *Velocity vectors and contours of the Y-component velocity on Z-X plane at 1.5-mm above the impingement surface for an array of impinging jets in a confined channel: (a) In-line arrangement and (b) Staggered arrangement (CFD results, the marked circles represent the position of the orifice).*

For case of the in-line arrangement, as shown in Fig. 14(a), the impingement region of each cell is more elongated in the downstream direction and contracted in the upstream direction as going downstream. This characteristic of flow pattern agrees with the flow visualization study of multiple jets [2], while the impingement regions for column No.5 and No.6 of the staggered arrangement could not be seen on the oil film footprint as shown in Fig. 14(b). This may due to strong mixing between jets and cross-flow before impingement on surface.

Schematic diagrams of cross-flow that flow through the array of impinging jets for the in-line and staggered arrangements are shown in Fig. 15. The cross-flow passes easily through channels between the rows of jets in the case of in-line arrangement, whereas cross-flow from a former column of impinging jets strongly exerts and interacts with the downstream impinging jets in the case of staggered arrangement.

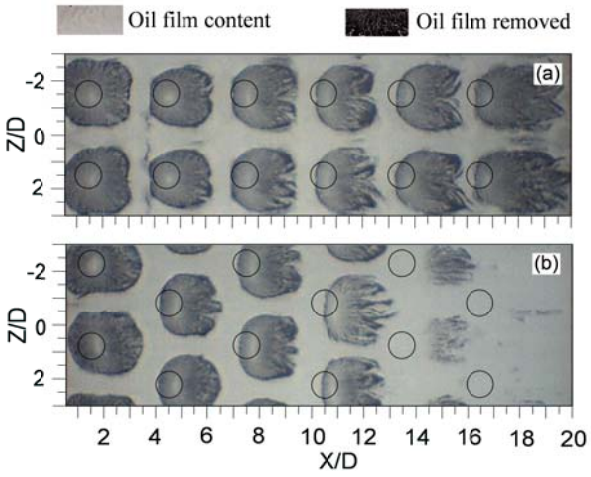

Fig. 14 *Oil film patterns on the impingement surface for an array of impinging jets in a confined channel: (a) In-line arrangement and (b) Staggered arrangement.*

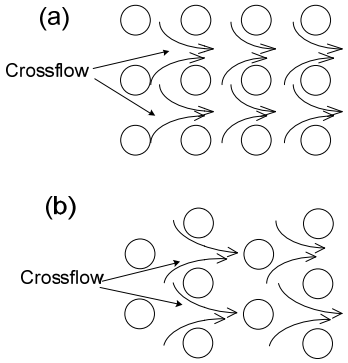

Fig. 15 *Cross-flow patterns through an array of impinging jets for different jet arrangements: (a) In-line arrangement and (b) Staggered arrangement.*

Thermal visualization on the impingement surface for array of impinging jets in confined channel are shown in Fig. 16. The color patterns of TLC sheet correspond to the flow patterns on the impingement surface in Fig. 15. In the figures, the green region is corresponding to impingement regions with high heat transfer rate. In case of the in-line arrangement, the impingement region shifted to downstream due to the deflection of impinging jet in cross-flow as shown in Fig. 16(a). The impingement region becomes smaller and changes its shape from circular to semi-circular because the jet mixing with cross-flow before impingement. The cross-flow effect becomes stonger and the displacement of the impingement region from orifice location is larger as it moves downstream.

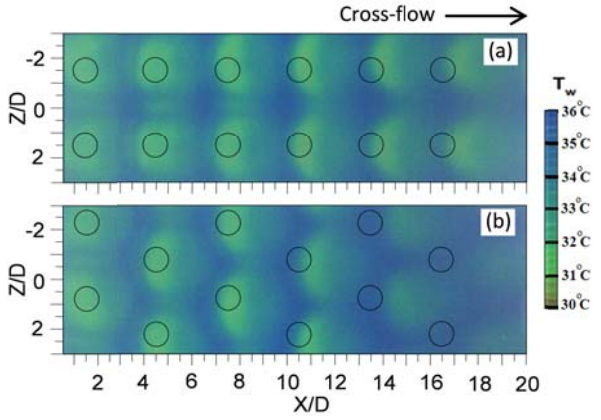

Fig. 16 *Thermal visualization on the impingement surface for an array of impinging jets in confined channel: (a) In-line arrangement and (b) Staggered arrangement (T_j=27 °C, $\dot{q}_{joule}$ = 429 W/m^2).*

For the case of staggered arrangement, the heat transfer rate for impingement region decreased as going downstream, particularly for impinging jets in column No. 5 and No. 6. The impingement regoins for this two columns are unclear. This is due to strong mixing between jet and cross-flow and loss momentum before impinging on surface.

Fig. 17 shows local Nusselt number distributions along X-axis direction on different line at Z/D=0, 1.5. For case of in-line arrangement, the peak Nusselt number at each impingement region increases continuously from column No.1 to column No.4 on line at Z/*D*=1.5. The highest peak Nusselt number takes place at column No.4 and the peak decreases again for columns No.5 and No.6. This result can be explained by the effect of cross-flow velocity on the jet impingement flow. The Nusselt number at the stagnation point in the case of in-line arrangement is increased by the interaction of cross-flow with moderate velocity on jet impingement. It can be attributed to the fact that the turbulence intensity of the jet is increased by the moderate velocity of the cross-flow. However, in the case of high cross-flow velocity, the jet is strongly mixed with the cross-flow, so the peak Nusselt number at stagnation region decreases due to low momentum of jet impinging on the surface. This characteristic of Nusselt number peak at stagnation regions agrees with the previous study [5]. While, the distribution of Nusselt number on line at Z/D=0 shows the peaks at location between the jet impingement regions which the wall jets from adjacent impinging jets collide. The peaks shifts downstream and decreases as it moves downstream.

For case of staggered arrangement, the Nusselt number distributions in the upstream region (columns No.1 - 3) are not much different when compared to the case of the in-line arrangement as shown in Fig. 17(b) at same downstream location. However, the Nusselt number decreases rapidly for the downstream regions (column No.4 to No.6) because of direct collision of high cross-flow velocity with the downstream impinging jets. So, the jets are strongly deflected downstream without impingement as previously mentioned. This results in apparently no impingement on surface in the last column of impinging jets as shown in Fig. 13(b) and Fig. 14(b).

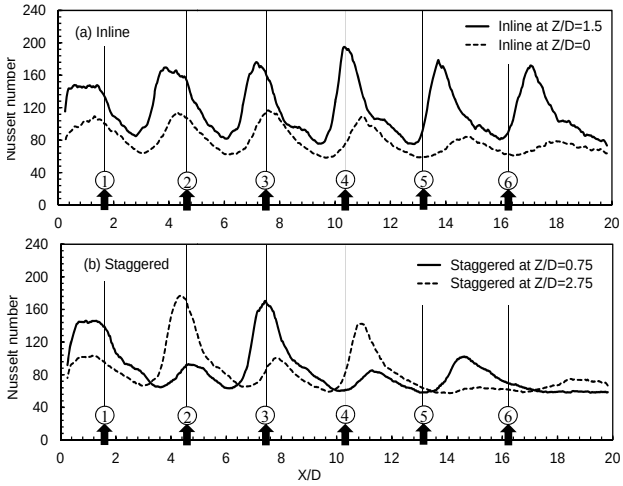

Fig. 17 *Local Nusselt number distributions along streamwise direction at Z/D=0, 1.5 (each arrow indicates the location of orifice): (a) In-line arrangement and (b) Staggered arrangement.*

Fig.18 compares spanwise average Nusselt number for an array of impinging jets in confined channel for in-line and staggered arrangement. The spanwise average Nusselt number was calculated from average temperature in spanwise direction at each downstream location X/D. It is found that the average Nusselt number for case of the staggered arrangement is lower than the case of the in-line arrangement from column No.3. This is as result of the small cross-flow effect. The cross-flow passes the channel between the rows of impinging jets for case of the in-line arrangement.

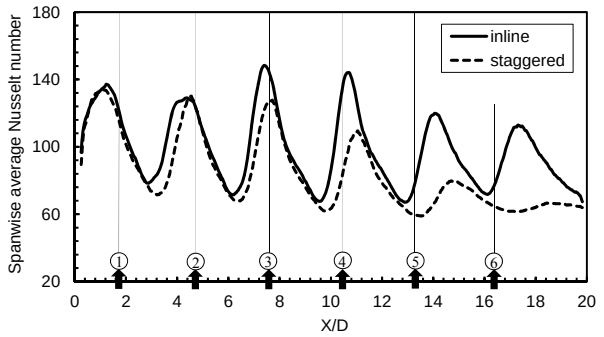

Fig.18 *Spanwise average Nusselt number for an array of impinging jets in confined channel (each arrow indicates the location of column jet).*

5. CONCLUDING REMARKS

In this study, the flow and heat transfer characteristics for a single impinging jet, a row of impinging jets and an array of impinging jets with a cross-flow effect were investigated for small jet-to-plate distance at H/D=2. The effect of the cross-flow velocity and jet arrangement were studied experimentally and numerically. The following conclusions could be drawn as follow:

1. For a single impinging jet with simulated cross-flow, the impingement region shifted to the downstream region and the shape of impingement region became semi-circular. This is due to the cross-flow deflecting and mixing with the jet before impingement. The cross-flow can enhance the heat transfer rate in the impingement region for the case of high cross-flow velocity at VR=3. This result is due to the high impingement velocity and high turbulence intensity near the impingement surface.

2. For a row of impinging jets, the displacement of impingement regions is larger than the case of a single impinging jet due to the blockage of row jets in cross-flow. The heat transfer enhancement was found in the downstream region of the impingement region when compared to the case of the single impinging jet. This is result of the circulation flows induced by the collision of wall jets from the adjacent impinging jets.

3. For an array of impinging jets, the effects of the cross-flow on the flow and heat transfer characteristics in the staggered arrangement are stronger than the case of the inline arrangement. The cross-flow can pass through the gaps between the rows of inline impinging jets, whereas the cross-flow was blocked by the downstream impinging jet in the case of staggered arrangement. The spanwise average Nusselt number for the case of the inline arrangement is higher than the case of the staggered arrangement, particularly for the downstream impinging jets.

REFERENCES

[1] R. Viskanta, Heat transfer to impinging isothermal gas and flame jets, Exp. Therm. Fluid Sci. 6 (1993) 111-134.

[2] L.-E. Brizzi, A. Bernard, J.-L. Bousgarbies, E. Dorignac and J.-J. Vullierme, Study of several impinging jets, J. Thermal Science 9 (2000) 217-223.

[3] B.P.E. Dano and J.A. Liburdy, Structure detection and analysis of non-circular impinging jets in a semi-confined array configuration, Exp. Therm. Fluid Sci. 31 (2007) 991-1003.

[4] L.W. Florschuetz, D.E. Metzger and C.R. Truman, Jet array impingement with cross-flow - correlation of streamwise resolved flow and heat transfer distributions, NASA Contractor Report 3373, Grant NSG-3075 (1981).

[5] V. Katti and S.V. Prabhu, Influence of spanwise pitch local heat transfer distribution for in-line arrays of circular jets with air flow in two opposite, Exp. Therm. Fluid Sci. 14 (2008) 84-95.

[6] J. M. M. Barata and D. F. G. Durao, Laser-doppler measurements of impinging jet flows through a cross-flow, Experiments in Fluids, 36 (2004) 665-674.

[7] R. J. Goldstein and I. Behbahani, Impingement of a circular jet with and without cross flow, International Journal of Heat and Mass Transfer, 25, (1982) 1377-1382.

[8] J. P. Bouchez and R. J. Goldstein, Impingement cooling from a circular jet in a cross flow, International Journal of Heat and Mass Transfer, 18, (1975) 719-730.

[9] M. Wae-hayee, P. Tekasakul, S. Eiamsa-ard and C. Nuntadusit, Effect of cross-flow velocity on flow and heat transfer characteristics of impinging jet with low jet-to-plate distance, Journal of Mechanical Science and Technology, xx (2014) xxx-xxx.

[10] M. Wae-hayee, P. Tekasakul, S. Eiamsa-ard and C. Nuntadusit, Flow and heat transfer characteristics of in-line impinging jets with cross-flow at short jet-to-plate distance, Experimental Heat Transfer, xx, (2014) xxxx-xxx.

[11] M. Wae-hayee, P. Tekasakul and C. Nuntadusit, Influence of nozzle arrangement on flow and heat transfer characteristics for arrays of circular impinging jets, Songklanakarin Journal of Science and Technology, 35 (2012) 203-212.

[12] N. Zuckerman and N. Lior, Jet impingement heat transfer: physics, correlations, and numerical modeling, Advances in Heat Transfer 39 (2006) 565-631.

[13] M. W. Heo, K. D. Lee and K. Y. Kim, Optimization of an inclined elliptic impinging jet with cross flow for enhancing heat transfer, *Heat and Mass Transfer,* 47 (2011) 731-742.

[14] T. T. Chandratilleke, D. Jagannatha and R. Narayanaswamy, Heat transfer enhancement in microchannels with cross-flow synthetic jets, International Journal Thermal Sciences, 49 (2010) 504-513.

[15] S. Ashforth-Frost and K. Jambunathan, Effect of nozzle geometry and semi-confinement on the potential core of a turbulent axisymmetric free jet, International Communication in Heat and Mass Transfer, 23 (1996) 155-162.

[16] S. Ashforth-Frost, K. Jambunathan and C. F. Whitney, Velocity and turbulence characteristics of a semiconfined orthogonally impinging slot jet, Experimental Thermal and Fluid Science, 14 (1997) 60-67.

[17] J. M. M. Barata, Fountain flows produced by multiple jets in a cross-flow. AIAA Journal, 34 (1996) 2523-2530.

[18] D. Ostheimer and Z. Yang, A CFD study of twin impinging jets in a cross-flow, The Open Numerical Methods Journal, 4 (2012) 24-34.

Makatar Wae-hayee is currrently Ph. D. candidate in Mechanical Engineerin g at the Department of Mechanical En gineering, Faculty of Engineering, Prin ce of Songkla University, Thailand. H e concerns in flow and heat transfer c haracteristics of impinging jets.

Perapong Tekasakul is an associate professor at the Department of Mechanical Engineering, Faculty of Engineering, Prince of Songkla University, Thailand. He received his Ph.D. from University of Missouri-Columbia, U.S.A., in 1996. His research focus includes computational fluid dynamics, heat transfer, solar drying, and atmospheric environment.

Chayut Nuntadusit is Assistant Professor of Mechanical Engineering at Prince of Songkla University, Thailand. He received Ph.D. at Osaka University in 2004. His current interests include heat transfer enhancement for jet impingement, jet flow control and optical measurement.